

# qReduMIS: A Quantum-Informed Reduction Algorithm for the Maximum Independent Set Problem

Martin J. A. Schuetz,<sup>1,2,\*</sup> Romina Yalovetzky,<sup>3,\*</sup> Ruben S. Andrist,<sup>1</sup> Grant Salton,<sup>1,2</sup> Yue Sun,<sup>3</sup> Rudy Raymond,<sup>3</sup> Shouvanik Chakrabarti,<sup>3</sup> Atithi Acharya,<sup>3</sup> Ruslan Shaydulin,<sup>3</sup> Marco Pistoia,<sup>3,†</sup> and Helmut G. Katzgraber<sup>1,†</sup>

<sup>1</sup>Amazon Advanced Solutions Lab, Seattle, Washington 98170, USA

<sup>2</sup>AWS Center for Quantum Computing, Pasadena, CA 91125, USA

<sup>3</sup>Global Technology Applied Research, JPMorgan Chase, New York, NY 10017 USA

(Dated: March 18, 2025)

We propose and implement a quantum-informed reduction algorithm for the maximum independent set problem that integrates classical kernelization techniques with information extracted from quantum devices. Our larger framework consists of dedicated application, algorithm, and hardware layers, and easily generalizes to the maximum weight independent set problem. In this hybrid quantum-classical framework, which we call qReduMIS, the quantum computer is used as a co-processor to inform classical reduction logic about frozen vertices that are likely (or unlikely) to be in large independent sets, thereby opening up the reduction space after removal of targeted subgraphs. We systematically assess the performance of qReduMIS based on experiments with up to 231 qubits run on Rydberg quantum hardware available through Amazon Braket. Our experiments show that qReduMIS can help address fundamental performance limitations faced by a broad set of (quantum) solvers including Rydberg quantum devices. We outline implementations of qReduMIS with alternative platforms, such as superconducting qubits or trapped ions, and we discuss potential future extensions.

## I. INTRODUCTION

The maximum independent set (MIS) problem is a paradigmatic, NP-hard combinatorial optimization problem with close ties to the well-known, complementary maximum clique and minimum vertex cover problems [1]. Practical applications can be found in virtually every industry, including computer vision [2], map labeling [3], network design [4], vehicle routing [5], and quantitative finance [6–8], to name a few. Given an undirected graph  $\mathcal{G} = (\mathcal{V}, \mathcal{E})$  with nodes  $\mathcal{V}$  and edges  $\mathcal{E}$ , an independent set is a subset  $\mathcal{I} \subseteq \mathcal{V}$ , such that no two vertices in the set  $\mathcal{I}$  share an edge. The goal of the MIS problem is to find an independent set  $\mathcal{I}$  with maximum cardinality. Such a set is called a *maximum independent set* of size  $|\text{MIS}| = |\mathcal{I}|$ . Similarly, for a weighted graph  $\mathcal{G} = (\mathcal{V}, \mathcal{E}, \omega)$  with vertex weight function  $\omega : \mathcal{V} \rightarrow \mathbb{R}^+$ , the generalized maximum weight independent set (MWIS) problem asks for an independent set  $\mathcal{I}$  with maximum weight  $\omega(\mathcal{I}) = \sum_{v \in \mathcal{I}} \omega(v)$ .

**Classical ReduMIS.** One of today’s leading heuristics for the MIS problem is the ReduMIS algorithm [9], which intermixes a suite of reduction (or kernelization) techniques with a heuristic evolutionary algorithm. Reduction techniques are polynomial time procedures that can shrink a given input graph to an irreducible kernel by removing well-defined subgraphs. These subgraphs are removed through targeted selection of exposed vertices that are provably part of some maximum(-weight) independent set, hence maintaining optimality [10–16]. Whenever an irreducible kernel is identified, ReduMIS

makes use of an evolutionary approach to identify and remove vertices that are likely part of a large independent set, thereby opening up yet again the reduction space for further kernelization. Ultimately, a solution to the MIS or MWIS problem on the original input graph can be found by undoing previously applied reductions, with numerical experiments reporting state-of-the-art results for both large MIS and MWIS problem instances [9, 17].

**Quantum optimization.** Over the last few decades, quantum optimization algorithms have emerged as a novel paradigm for solving combinatorial optimization problems, such as the MIS problem [18]. Prominent examples include quantum annealing algorithms (QAA) [19–23] and the quantum approximate optimization algorithm (QAOA) [24, 25]. In particular, analog neutral-atom quantum machines in the form of Rydberg atom arrays have attracted broad interest as a novel class of programmable and scalable special-purpose quantum devices that can natively encode and (approximately) solve the MIS (and MWIS) problem on unit-disk (UD) graphs [26–34]. Recent QAA-based experiments report on a potential super-linear quantum speedup over classical simulated annealing [29, 35]. However, for a broad set of Markov-chain Monte Carlo algorithms, the same experiments also show that the algorithmic performance is suppressed exponentially in the conductance-like hardness parameter  $\mathbb{H}$ , defined as  $\mathbb{H} = D_{|\text{MIS}|-1} / (|\text{MIS}| \cdot D_{|\text{MIS}|})$ , where  $D_\alpha$  denotes the degeneracy of the independent sets of size  $\alpha$ . Specifically, the success probability to find the MIS in a single algorithmic run (shot), denoted as  $P_{\text{MIS}}$ , is shown to follow the form  $P_{\text{MIS}} \approx 1 - \exp(-C\mathbb{H}^{-\beta})$  [29], where  $\beta$  depends on details of the given algorithm, and  $C$  refers to a positive (fitted) constant.

**Quantum ReduMIS (qReduMIS).** In this work we propose and implement a novel quantum-informed algo-

\*These authors contributed equally.

†These authors acted as Co-PIs.

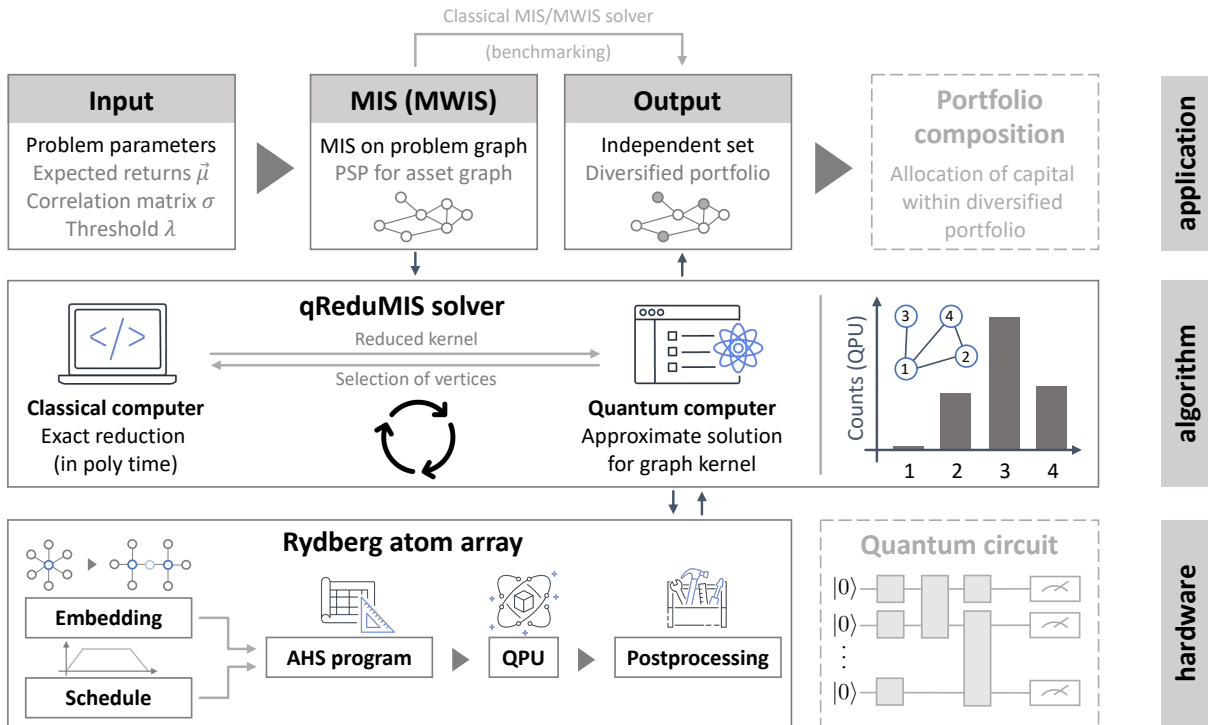


FIG. 1: Schematic illustration of the hybrid qReduMIS framework, with distinct (i) application, (ii) algorithm, and (iii) hardware layers (from top to bottom). The application layer is illustrated for an example portfolio selection problem (PSP) that can be framed as a MIS (or MWIS) problem on an asset graph, the solution to which can be fed into a downstream portfolio composition problem. For a given problem instance on a graph  $\mathcal{G}$ , the qReduMIS algorithm solves the MIS problem by intermixing exact, polynomial time reduction logic with information obtained from quantum measurements to unblock the kernelization process whenever necessary by identifying and removing frozen vertices that have a high (or low) likelihood to be part of large independent sets. The qReduMIS framework is hardware-agnostic, and can be powered by both *digital* or *analog* quantum devices, such as Rydberg atom arrays implementing analog Hamiltonian simulation (AHS) programs.

rithm (dubbed *qReduMIS*), which integrates exact classical kernelization with a quantum processing unit (QPU) used as co-processor (rather than a classical evolutionary heuristic) that unblocks the reduction process whenever necessary; see Fig. 1 for a schematic illustration. The algorithm is hardware-agnostic and embedded in a larger, three-tiered framework, with distinct application, algorithm, and hardware layers. By design, the algorithm leans heavily on classical kernelization, and periodically leverages information obtained from QPU measurements to unblock the kernelization process by identifying and removing frozen vertices that have a high (or low) likelihood to be part of large independent sets. This offers several benefits: First, classical kernelization is provably optimal, second these methods are fast (e.g., linear-time for sparse graphs), and third, kernelization methods are insensitive to the hardness parameter  $\mathbb{H}$  [36].

## II. qReduMIS METHODOLOGY

In the following, we outline the anatomy of qReduMIS in more detail, systematically stepping through its individual layers from application, to algorithm, to hardware

layers (cf. Fig. 1 from top to bottom).

**Application layer.** The qReduMIS algorithm accepts generic MIS instances as problem input and can be extended to MWIS instances by combining generalized reduction techniques for MWIS [17] with quantum devices compatible with the MWIS problem [37, 38]. Generically, in the application layer we construct a MIS / MWIS problem instance for a given set of problem-specific input parameters. The corresponding problem graph is fed to the algorithm layer which then returns a (large) independent set that can be further processed based on the underlying use case. For illustration, in Fig. 1 we showcase the application layer with an example portfolio selection problem (PSP). Given information from historical stock price data in the form of expected returns  $\mu$  and inter-asset correlations  $\sigma$ , together with a user-defined correlation threshold  $\lambda$ , the PSP can be framed as an MIS (or MWIS) problem on a so-called asset (or market) graph [7, 8, 39], which is passed to the algorithm layer. The output solution represents a diversified portfolio within a larger universe of assets which can be integrated into a larger multi-stage portfolio management pipeline where portfolio selection is followed by portfolio composition [8].

---

**Algorithm 1** Basic Structure of qReduMIS
 

---

**Input** graph  $G = (V, E)$ , RCL size  $K_{\text{RCL}}$ , selection parameter  $\lambda$  # default  $K_{\text{RCL}} = \lambda = 1$   
**Global**  $\mathcal{W} = \emptyset, \mathcal{S} = \emptyset, \mathcal{R} = \emptyset$  # best solution (incumbent), set of selected nodes, set of removed nodes  
 # Set up selection scheme  
 params = {size :  $\lambda$ , RCLsize :  $K_{\text{RCL}}$ , strategy :  $in$ }  
**Procedure** qReduMIS( $G$ )  
   **if**  $G$  is empty **then return**  $\mathcal{W}$   
   # Get kernel, selected, and removed nodes  
    $(\mathcal{K}, s, r) \leftarrow \text{CLASSICALREDUCE}(G)$   
   Append  $s$  to  $\mathcal{S}$ , append  $r$  to  $\mathcal{R}$   
   **if**  $\mathcal{K}$  is empty **then update and return**  $\mathcal{W}$   
   # Get candidate sets for kernel from QPU  
    $\{\mathcal{I}_n\} \leftarrow \text{QUANTUMMIS}(\mathcal{K})$   
   # Update incumbent  
   **if**  $|\mathcal{S}| + \max(|\mathcal{I}_n|) > |\mathcal{W}|$  **then update**  $\mathcal{W}$   
   # Select  $\lambda$  frozen (fixed) nodes with "in/out" strategy,  
   # and update  $\mathcal{S}$  and  $\mathcal{R}$  accordingly  
    $(\mathcal{Q}, s_q, r_q) \leftarrow \text{SELECT}(\{\mathcal{I}_n\}, \text{params})$   
   Append  $s_q$  to  $\mathcal{S}$ , append  $r_q$  to  $\mathcal{R}$   
    $\mathcal{K}' \leftarrow \mathcal{K}[\mathcal{V}_{\mathcal{K}} \setminus \mathcal{Q}]$  # Get updated (inexact) kernel  
   qReduMIS( $\mathcal{K}'$ ) # Recurse on inexact kernel  
**return**  $\mathcal{W}$

---

**Algorithm layer.** The algorithm layer is at the center of the qReduMIS framework, involving both classical and quantum resources, with the QPU feeding information to the classical reduction logic in every iteration of the algorithm. See Algorithm 1 for a basic outline of the core routine. While several variants of qReduMIS are conceivable, ranging from greedy heuristics to exact branch-and-reduce-type algorithms, here we focus on a semi-greedy implementation thereof. Independent of implementation details, qReduMIS comprises three core modules, given by (i) CLASSICALREDUCE( $\cdot$ ), (ii) QUANTUMMIS( $\cdot$ ), and (iii) SELECT( $\cdot$ ) methods.

The CLASSICALREDUCE routine takes a graph  $\mathcal{G}$  as input and outputs a smaller graph kernel  $\mathcal{K}$ , along with sets of nodes that have been selected or removed, respectively. To achieve this reduction, one can draw from the full suite of reduction procedures developed over the last two decades [9, 16, 40], involving, for example, techniques such as isolated vertex removal [10], vertex folding [41], or critical independent set reductions [11]. For definiteness, here we leverage a simple, yet efficient reduction procedure known as isolated vertex removal [10, 13, 36], which makes use of the notion of exposed corner nodes (also known as isolated or simplicial vertices) that are provably part of some MIS/MWIS by a simple cut-and-paste argument [10, 13, 15, 36]. By iteratively selecting those corner nodes and removing their neighborhood, this simple kernelization technique is able to efficiently shrink a given input graph  $\mathcal{G}$  to an irreducible kernel  $\mathcal{K}$ —typically in linear time—while preserving optimality [36].

Next, the irreducible kernel  $\mathcal{K}$  is passed to the QUANTUMMIS routine, which samples from the low-energy sector and computes high-quality solutions in the form of independent sets  $\{\mathcal{I}_n\}$  for the kernel, for

$n = 1, \dots, n_{\text{shots}}$ , with  $n_{\text{shots}}$  referring to the number of QPU measurements (shots). As further detailed below, both analog (i.e., quantum annealing type) or digital (i.e., circuit-based) quantum devices can be called in the backend to compute these independent sets. In the case that the kernel's size exceeds the QPU's capabilities, qubit compression [42], lightcone [43], or decomposition techniques [44] may be used to effectively shrink the problem size and enable the use of near-term quantum devices.

Finally, the SELECT routine takes the QPU's output  $\{\mathcal{I}_n\}$  as input, and leverages its inherent sampling capabilities to identify frozen nodes that tend to be included in independent sets (or excluded), across all measurements (or some suitably filtered version thereof). See the histogram in Fig. 1 for a simple example with four nodes in which node 1 is never part of a low-energy solution, while node 3 is always selected (across different MIS solutions). In this case, both nodes 1 and 3 are *frozen*. In the context of superconducting annealers, this concept has been introduced as *sample persistence* [45], which amounts to the evaluation of one-point correlations sourced from a low-energy (quantum) state, but can be generalized to higher-order correlations [33, 46]. Here, we consider two simple selection mechanisms, both based on a histogram of in-set selection counts across all nodes  $i = 1, \dots, |\mathcal{V}_{\mathcal{K}}|$ , as can be straightforwardly sourced from the measurement results  $\{\mathcal{I}_n\}$ ; compare Fig. 1 for a toy illustration. We refer to *in-set* (*out-set*) nodes as those vertices which have the highest (lowest) count numbers, respectively, representing their likelihood to be part of high-quality independent set solutions. In a semi-greedy implementation of qReduMIS, we randomly pick  $\lambda$  candidate nodes from a restricted candidate list (RCL) of size  $K_{\text{RCL}}$  that tracks those nodes with the highest (lowest) counts, possibly with a bias towards low-degree nodes for in-set nodes, simply because high-degree vertices are unlikely to be in a large independent set [9]. The nodes identified from the RCL are then used to construct a set  $\mathcal{Q}$  to remove from the kernel. For the out-set strategy,  $\mathcal{Q}$  contains the  $\lambda$  randomly-selected nodes, whereas for the in-set strategy  $\mathcal{Q}$  contains the  $\lambda$  randomly-selected nodes *and* their neighbors. After this quantum-informed elimination of  $\mathcal{Q}$ , we repeat the procedure on the updated kernel  $\mathcal{K}' \leftarrow \mathcal{K}[\mathcal{V}_{\mathcal{K}} \setminus \mathcal{Q}]$ , with the central idea that the quantum-informed removal of  $\mathcal{Q}$  once again opens up the reduction space for further classical kernelization and helps guide the algorithm towards an MIS solution.

**Hardware layer.** The qReduMIS hardware layer can involve hardware solvers such as Ising machines [47], and analog or digital quantum devices. Specifically, quantum algorithms such as QAA [19–23] or QAOA [24, 25] run on quantum devices can be used to prepare a superposition of low-energy candidate solutions to the MIS/MWIS problem from which information is extracted upon measurement to unblock classical kernelization.

Given a graph  $\mathcal{K} = (\mathcal{V}_{\mathcal{K}}, \mathcal{E}_{\mathcal{K}})$ , the MIS problem is equivalent to finding the ground state of the classical Hamil-

tonian

$$H(\mathbf{n}) = - \sum_{i \in \mathcal{V}_K} n_i + U \sum_{(i,j) \in \mathcal{E}_K} n_i n_j, \quad (1)$$

with  $U > 1$  and  $n_i = 1$  if node  $i$  is in the set (and  $n_i = 0$  otherwise); generalization to the MWIS problem is straightforward. Introducing the Ising spin variables  $z_i = 2n_i - 1$  and promoting those to Pauli spin operators  $z_i \rightarrow \hat{Z}_i$  we obtain the corresponding MIS *quantum* Ising Hamiltonian

$$\hat{H}_{\text{cost}} = \sum_{i,j} J_{ij} \hat{Z}_i \hat{Z}_j + \sum_i h_i \hat{Z}_i, \quad (2)$$

with local fields  $h_i$  and couplers  $J_{ij}$ . The common theme across different quantum algorithms and hardware platforms is then to prepare a quantum many-body system undergoing coherent, programmable dynamics, as described by the unitary evolution

$$|\Psi(\theta)\rangle = \mathcal{U}(\theta)|\Psi_{\text{initial}}\rangle, \quad (3)$$

which seeks to prepare  $|\Psi(\theta)\rangle$  via control parameters  $\theta$  as to minimize the expectation value with respect to the cost Hamiltonian  $\hat{H}_{\text{cost}}$ . The unitary  $\mathcal{U}(\theta)$  can be engineered with both analog and digital quantum devices, across hardware platforms such as superconducting qubits or trapped ions, as further detailed in Appendix A 2. In the following, we focus on implementations based on Rydberg atom arrays.

Given the ability of Rydberg atom arrays to efficiently encode MIS (and MWIS) problems on unit-disk graphs [26, 29], here we focus on qReduMIS backed by Rydberg atom arrays. See Fig. 1 for a schematic illustration of our end-to-end workflow for solving the MIS with analog Hamiltonian simulation (AHS) programs run on Rydberg QPUs. In this setup, each atom represents a vertex, and coherent excitation from an atom's ground state  $|0\rangle$  into an excited Rydberg state  $|1\rangle$  can be utilized for hardware-efficient encoding of unit-disk MIS problems, with the Rydberg blockade mechanism effectively inducing edges within the (tunable) unit-disk radius  $R_b \sim 1 - 10 \mu\text{m}$  [48–51]. The quantum dynamics of Rydberg atom arrays is described by the Hamiltonian  $\hat{H} = \hat{H}_{\text{mix}} + \hat{H}_{\text{cost}}$ , with ( $\hbar = 1$ )

$$\begin{aligned} \hat{H}_{\text{mix}} &= \frac{\Omega(t)}{2} \sum_i \left( e^{i\phi(t)} |0\rangle_i \langle 1| + \text{h.c.} \right), \\ \hat{H}_{\text{cost}} &= -\Delta(t) \sum_i \hat{n}_i + \sum_{i < j} V_{ij} \hat{n}_i \hat{n}_j, \end{aligned} \quad (4)$$

where  $\hat{n}_i := |1\rangle_i \langle 1|$  is the occupation number operator for atom  $i$ ,  $V_{ij} = C_6 / \|\mathbf{x}_i - \mathbf{x}_j\|^6$  for atoms at positions  $\mathbf{x}_i$  and  $\mathbf{x}_j$ , respectively, and  $C_6$  is the van der Waals coefficient. Here,  $\theta(t) = \{\Omega(t), \phi(t), \Delta(t)\}$  specifies a programmable schedule in terms of the global Rabi frequency  $\Omega(t)$ , the phase of the Rabi drive  $\phi(t)$ , and laser detuning  $\Delta(t)$ . Together with a two-dimensional atom

TABLE I: Average success probabilities  $P_{\text{MIS}}$  achieved with QAA and qReduMIS (with in-set selection strategy) using the QuEra Aquila QPU for four test instances (all with  $n = 137$  vertices) referenced by their hardness parameters  $\mathbb{H}$ . More details can be found in Appendix B.

| Instance hardness $\mathbb{H}$ | $\sim 1.478$ | $\sim 14.12$ | $\sim 125.5$ | $\sim 1435$ |
|--------------------------------|--------------|--------------|--------------|-------------|
| QAA                            | 35.2%        | 0.8%         | 0.7%         | 0%          |
| QAA (Ref. [34])                | 47.8%        | 0.4%         | 1.9%         | 0%          |
| qReduMIS                       | 100%         | 100%         | 100%         | 100%        |

arrangement  $\{\mathbf{x}_i\}$ ,  $\theta(t)$  defines a complete AHS program for quantum devices available online today with up to 256 qubits [52]. Neglecting corrections from Rydberg interaction tails and carefully choosing positive detuning  $\Delta_{\text{UB}} > \Delta > \Delta_{\text{LB}} > 0$  [34], it is straightforward to see that  $\hat{H}_{\text{cost}}$  in Eq. (4) can capture the MIS cost function in Eq. (1) on unit-disk graphs, in a quantum system with  $n_i \rightarrow \hat{n}_i$ , while the driver  $\hat{H}_{\text{mix}}$  allows to coherently drive transitions between bit strings [26]. Generalized MWIS instances can be tackled using *local* detuning capabilities, effectively taking  $\Delta(t) \rightarrow \Delta_i(t)$  [37, 38]. If a given problem instance does not match the unit-disk connectivity supported natively by the hardware, we resort to embedding schemes, as described in Refs. [36, 37], that map the logical input to a physical graph compatible with the hardware connectivity constraints, typically at the expense of a quadratic overhead in the required number of qubits. At the end of the schedule, site-resolved projective measurements can be used to read out the final quantum many-body state. Given this raw output, we use simple post-processing logic that repairs potential violations of the independence constraint and ensures the feasibility of all solution candidates [29]. Out-set (in-set) nodes to be considered for selection per SELECT method then manifest as frozen (persistent) vertices for which the local observables  $\hat{n}_i$  have low (high) expectation values, i.e.,  $\langle \hat{n}_i \rangle \approx 0$  ( $\langle \hat{n}_i \rangle \approx 1$ ), as those give the probability to measure the  $i$ -th atom in the Rydberg state  $|1\rangle$  at the end of the anneal.

**qReduMIS run time.** Unless a maximum number of iterations is specified, qReduMIS proceeds until the kernel is empty. We denote the number of iterations needed to fully reduce the kernel by  $D$ . Every iteration involves both classical ( $\tau_{\text{cl}}$ ) as well as quantum processing time ( $\tau_{\text{q}}$ ), up to the last step that only involves classical kernelization. Considering realistic wall-clock times, we have  $\tau_{\text{cl}} \ll \tau_{\text{q}}$ , leading to a total run time  $T \approx D \cdot n_{\text{shots}} \tau$ , with  $\tau_{\text{q}} = n_{\text{shots}} \tau$  and hardware-dependent cycle time  $\tau$ . For current Rydberg devices,  $\tau$  is limited by (destructive) blow-out measurement techniques to  $\tau \sim 0.1\text{s}$  [52]. For typical input graphs with  $n \sim 1000$  nodes, we estimate  $D \lesssim 10$ , based on repeated classical kernelization, leading to  $T \approx 100\text{s} - 1000\text{s}$  for  $n_{\text{shots}} \approx 100 - 1000$  measurements per iteration. This timescale can be reduced via faster cycle times through improved reload-



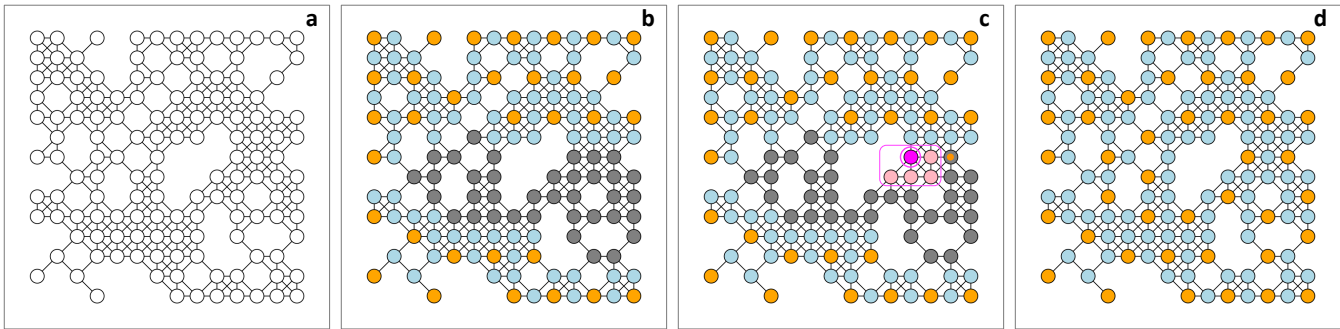


FIG. 2: Snapshots of the qReduMIS algorithm (with in-set selection strategy) for the hardest instance listed in Tab. I with  $\mathbb{H} \sim 1435$ . (a) The problem input is given in terms of a site-diluted union-jack graph with  $n = 137$  nodes on a square lattice of side length  $L = 14$ . (b) qReduMIS first calls CLASSICALREDUCE. Orange nodes are selected ( $n_i = 1$ ), blue nodes are removed ( $n_i = 0$ ) per kernelization, until an irreducible kernel  $\mathcal{K}$  is found, with 37 kernel nodes displayed in dark gray. (c) Next, the QPU is called to unblock the reduction procedure. Solution candidates for the kernel are sampled, and the node highlighted in pink is identified as a frozen node with high in-set probability. Selection of this node and removal of its kernel neighborhood (pink box) results in an updated kernel  $\mathcal{K}'$  that features an exposed corner node (highlighted with an orange dot). (d) The remaining kernel is fully reducible. Within two iterations (with two calls to CLASSICALREDUCE and one quantum-informed selection) qReduMIS finds an optimal solution of size  $|\text{MIS}| = 45$ .

ing schemes [52], the ability to parallelize measurements across a single QPU device provided both enough space and qubits are available [52], and the potential to parallelize the workload across multiple QPUs, if available.

### III. NUMERICAL EXPERIMENTS

We now assess the performance of qReduMIS experimentally. For the sake of a well-controlled testbed, we focus on hardware-native instances, foregoing the requirement for excessive compilation. In particular, we consider (non-planar) random union-jack (UJ) instances, as previously studied in, e.g., Refs. [29, 32, 35, 53]. We compare the performance of QAA vs a semi-greedy implementation of qReduMIS with in-set selection strategy and 20 classical shots per instance, for the same optimized schedule [34], and  $n_{\text{shots}} = 1000$  throughout. We provide results based on experiments run on the QuEra Aquila QPU available on Amazon Braket [52]. We apply post-processing logic that repairs violations of the independence constraint [29, 52]. We also perform post-selection and only consider those shots for which the lattice has been correctly filled with atoms, as done in Ref. [34].

**Example instances.** We first focus on four example instances with  $n = 137$  nodes and hardness ranging from  $\mathbb{H} \sim 1.478$  to  $\mathbb{H} \sim 1435$ , as previously studied in Refs. [32] and [34]. In line with the expected strong performance dependence on  $\mathbb{H}$ ,  $P_{\text{MIS}} \approx 0.478$ ,  $P_{\text{MIS}} \approx 0.004$ ,  $P_{\text{MIS}} \approx 0.019$ , and  $P_{\text{MIS}} = 0$  has been reported for those four instances, using the optimized QAA developed in Ref. [34]. Our results are given in Tab. I. To illustrate the anatomy of qReduMIS, in Fig. 2 we provide snapshots of the algorithm for one particular instance, showing how the algorithm can succeed in finding an MIS through repeated rounds of kernelization guided by information ex-

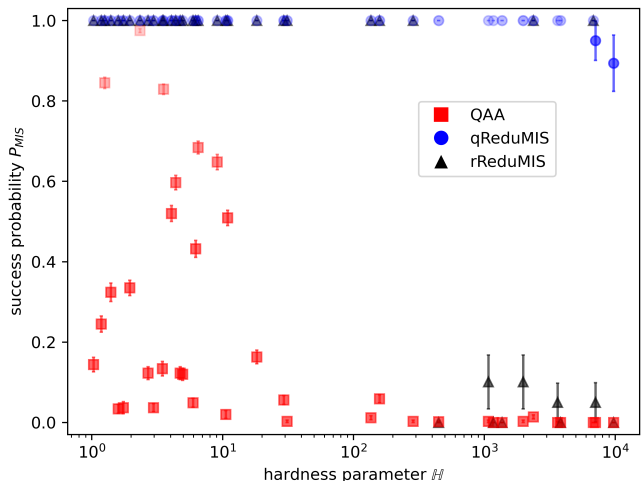


FIG. 3: Success probability  $P_{\text{MIS}}$  as a function of the hardness parameter  $\mathbb{H}$ , for QAA (red squares), qReduMIS (blue circles), and a random-informed baseline (black triangles). Error bars refer to 90% confidence intervals as extracted via bootstrapping.

tracted from quantum measurements. Overall, we find that qReduMIS outperforms QAA on all four instances, reaching  $P_{\text{MIS}} = 1$  on all four instances, including the hardest instance for which QAA fails to find the MIS [34], i.e.,  $P_{\text{MIS}} = 0$ .

**Systematic experiments.** Next, we perform systematic experiments on a larger set of 39 random UJ instances, with hardness parameters ranging over four orders of magnitude from  $\mathbb{H} \sim 1.03$  up to  $\mathbb{H} \sim 9717$ , based on graphs with  $n = 7 - 231$  nodes. To validate the usefulness of the quantum information in guiding the kernelization process, we also consider a simple *random-*

*informed* baseline (dubbed rReduMIS), in which in-set nodes are chosen randomly from the kernel. Our results are displayed in Fig. 3. As expected, for QAA  $P_{\text{MIS}}$  is strongly suppressed for hard instances, dropping to small  $P_{\text{MIS}} \gtrsim 0$  for most instances with  $\mathbb{H} \gtrsim 10$ . Conversely, qReduMIS solves most instances to optimality with  $P_{\text{MIS}} = 1$  and maintains a non-zero success rate with average  $P_{\text{MIS}} \gtrsim 89\%$  throughout the testbed. We also see that qReduMIS outperforms the random baseline rReduMIS, showing that the information extracted from the quantum backend does carry useful information. While  $P_{\text{MIS}} = 1.0$  for all instances with  $\mathbb{H} \lesssim 10^3$ , we find  $P_{\text{MIS}} \sim 0.89 - 0.95$  (on average) for two hard instances with  $\mathbb{H} \gtrsim 10^3$ , which we attribute to sub-optimal information sourced from the quantum sampler for relatively large (and, thus, harder) kernels; see Appendix B for further details. Ultimately, those performance drops may be addressed with extended reduction techniques [16] and (kernel) samplers that are insensitive to the hardness parameter, as discussed in Ref. [35], which we leave for future research. Still, given that the performance of qReduMIS is imperfect ( $P_{\text{MIS}} < 1$ ) only for those instances where QAA fails ( $P_{\text{MIS}} = 0$ ), for our testbed we find an optimal area-under-the-curve performance boost for  $P_{\text{MIS}}(\text{qReduMIS})/P_{\text{MIS}}(\text{QAA})$ .

#### IV. CONCLUSION AND OUTLOOK

In summary we have proposed and analyzed a family of quantum-informed reduction algorithms for the MIS-/MWIS problems (dubbed qReduMIS) in which exact kernelization is applied in tandem with a quantum co-processor that helps guide the repeated reduction process through the identification of frozen vertices. The qReduMIS algorithm is hardware-agnostic and embedded in a three-tier framework with distinct application, algorithm, and hardware layers. Our experiments with up to 231 qubits show that qReduMIS can help overcome fundamental performance limitations faced by (neutral atom) quantum processors. In future work it will be in-

teresting to integrate backtracking techniques [33] and expand the classical reduction toolkit [16]. Furthermore, one could integrate qubit compression [42], lightcone [43], or decomposition techniques [44], with the goal to study larger problem sizes, and run larger benchmarking experiments (e.g., comparing qReduMIS against classical ReduMIS) using a variety of hardware platforms such as superconducting qubits or trapped ions.

#### Acknowledgments

We thank Victor Bocking, Yaroslav Kharkov, Peter Komar, Lou Romano, Peter Sceusa, Alexander Buts, Jacob Albus, Pragna Subrahmanya, and Rajagopal Ganesan for their support. H.G.K. would like to thank Charlie Gatograbber for support during the final stages of writing this manuscript.

#### Disclaimer

This paper was prepared for informational purposes with contributions from the Global Technology Applied Research center of JPMorgan Chase & Co. This paper is not a product of the Research Department of JPMorgan Chase & Co. or its affiliates. Neither JPMorgan Chase & Co. nor any of its affiliates makes any explicit or implied representation or warranty and none of them accept any liability in connection with this paper, including, without limitation, with respect to the completeness, accuracy, or reliability of the information contained herein and the potential legal, compliance, tax, or accounting effects thereof. This document is not intended as investment research or investment advice, or as a recommendation, offer, or solicitation for the purchase or sale of any security, financial instrument, financial product or service, or to be used in any way for evaluating the merits of participating in any transaction.

- 
- [1] M. R. Garey and D. S. Johnson, *Computers and intractability; A guide to the theory of NP-completeness* (W. H. Freeman & Co., USA, 1990), ISBN 0716710455.
  - [2] T. A. Feo, M. G. C. Resende, and S. H. Smith, *A greedy randomized adaptive search procedure for maximum independent set*, *Operations Research* **42**, 860 (1994), URL <https://doi.org/10.1287/opre.42.5.860>.
  - [3] A. Gemsa, M. Nöllenburg, and I. Rutter, *Evaluation of labeling strategies for rotating maps*, *ACM J. Exp. Algorithmics* **21** (2016), ISSN 1084-6654, URL <https://doi.org/10.1145/2851493>.
  - [4] W. K. Hale, *Frequency assignment: Theory and applications*, *Proceedings of the IEEE* **68**, 1497 (1980).
  - [5] Y. Dong, A. V. Goldberg, A. Noe, N. Parotsidis, M. G. C. Resende, and Q. Spaen, *A metaheuristic algorithm for large Maximum Weight Independent Set problems* (2022), arXiv:2203.15805.
  - [6] V. Boginski, S. Butenko, and P. M. Pardalos, *Statistical analysis of financial networks*, *Computational Statistics and Data Analysis* **48**, 431 (2005).
  - [7] A. Kalra, F. Qureshi, and M. Tisi, *Portfolio asset identification using graph algorithms on a Quantum Annealer*, SSRN (2018), URL <https://ssrn.com/abstract=3333537>.
  - [8] R. Hidaka, Y. Hamakawa, J. Nakayama, and K. Tatumura, *Correlation-diversified portfolio construction by finding maximum independent set in large-scale market graph*, *IEEE Access* **11**, 142979 (2023).

- [9] S. Lamm, P. Sanders, C. Schulz, D. Strash, and R. F. Werneck, *Finding near-optimal independent sets at scale*, Journal of Heuristics **23**, 207 (2017), URL <https://doi.org/10.1007/s10732-017-9337-x>.
- [10] S. Butenko, P. Pardalos, I. Sergienko, V. Shylo, and P. Stetsyuk, in *Proceedings of the 2002 ACM Symposium on Applied Computing* (Association for Computing Machinery, New York, NY, USA, 2002), SAC '02, pp. 542–546, ISBN 1581134452, URL <https://doi.org/10.1145/508791.508897>.
- [11] S. Butenko and S. Trukhanov, *Using critical sets to solve the maximum independent set problem*, Operations Research Letters **35**, 519 (2007), ISSN 0167-6377, URL <https://www.sciencedirect.com/science/article/pii/S0167637706000952>.
- [12] S. Butenko, P. Pardalos, I. Sergienko, V. Shylo, and P. Stetsyuk, *Estimating the size of correcting codes using extremal graph problems* (Springer New York, New York, NY, 2009), pp. 227–243, ISBN 978-0-387-98096-6, URL [https://doi.org/10.1007/978-0-387-98096-6\\_12](https://doi.org/10.1007/978-0-387-98096-6_12).
- [13] D. Strash, in *Computing and Combinatorics*, edited by T. N. Dinh and M. T. Thai (Springer International Publishing, Cham, 2016), pp. 345–356, ISBN 978-3-319-42634-1.
- [14] L. Chang, W. Li, and W. Zhang, in *Proceedings of the 2017 ACM International Conference on Management of Data* (Association for Computing Machinery, New York, NY, USA, 2017), SIGMOD '17, pp. 1181–1196, ISBN 9781450341974, URL <https://doi.org/10.1145/3035918.3035939>.
- [15] D. Hespe, C. Schulz, and D. Strash, *Scalable kernelization for maximum independent sets*, ACM J. Exp. Algorithmics **24** (2019), ISSN 1084-6654, URL <https://doi.org/10.1145/3355502>.
- [16] E. Großmann, K. Langedal, and C. Schulz, *A comprehensive survey of data reduction rules for the maximum weighted independent set problem* (2024), 2412.09303, URL <https://arxiv.org/abs/2412.09303>.
- [17] E. Großmann, S. Lamm, C. Schulz, and D. Strash, in *Proceedings of the Genetic and Evolutionary Computation Conference* (Association for Computing Machinery, New York, NY, USA, 2023), GECCO '23, pp. 293–302, ISBN 9798400701191, URL <https://doi.org/10.1145/3583131.3590353>.
- [18] A. Abbas, A. Ambainis, B. Augustino, A. Bärtshi, H. Buhrman, C. Coffrin, G. Cortiana, V. Dunjko, D. J. Egger, B. G. Elmegreen, et al., *Challenges and opportunities in quantum optimization*, Nature Reviews Physics **6**, 718 (2024), URL <https://doi.org/10.1038/s42254-024-00770-9>.
- [19] T. Kadowaki and H. Nishimori, *Quantum annealing in the transverse ising model*, Phys. Rev. E **58**, 5355 (1998), URL <https://link.aps.org/doi/10.1103/PhysRevE.58.5355>.
- [20] E. Farhi, J. Goldstone, S. Gutmann, and M. Sipser, *Quantum computation by adiabatic evolution* (2000), arXiv:quant-ph/0001106.
- [21] E. Farhi, J. Goldstone, S. Gutmann, J. Lapan, A. Lundgren, and D. Preda, *A quantum adiabatic evolution algorithm applied to random instances of an np-complete problem*, Science **292**, 472 (2001), URL <https://www.science.org/doi/abs/10.1126/science.1057726>.
- [22] A. Das and B. K. Chakrabarti, *Colloquium: Quantum annealing and analog quantum computation*, Rev. Mod. Phys. **80**, 1061 (2008), URL <https://link.aps.org/doi/10.1103/RevModPhys.80.1061>.
- [23] P. Hauke, H. G. Katzgraber, W. Lechner, H. Nishimori, and W. Oliver, *Perspectives of quantum annealing: methods and implementations*, Rep. Prog. Phys. **83**, 054401 (2020).
- [24] E. Farhi, J. Goldstone, and S. Gutmann, *A quantum approximate optimization algorithm* (2014), arXiv:1411.4028.
- [25] L. Zhou, S.-T. Wang, S. Choi, H. Pichler, and M. D. Lukin, *Quantum Approximate Optimization Algorithm: Performance, mechanism, and implementation on near-term devices*, Phys. Rev. X **10**, 021067 (2020), URL <https://link.aps.org/doi/10.1103/PhysRevX.10.021067>.
- [26] H. Pichler, S.-T. Wang, L. Zhou, S. Choi, and M. D. Lukin, *Quantum optimization for Maximum Independent Set using Rydberg atom arrays* (2018), arXiv:1808.10816.
- [27] H. Pichler, S.-T. Wang, L. Zhou, S. Choi, and M. D. Lukin, *Computational complexity of the Rydberg Blockade in two dimensions* (2018), arXiv:1809.04954.
- [28] M. F. Serret, B. Marchand, and T. Ayril, *Solving optimization problems with Rydberg analog quantum computers: Realistic requirements for quantum advantage using noisy simulation and classical benchmarks*, Phys. Rev. A **102**, 052617 (2020), URL <https://link.aps.org/doi/10.1103/PhysRevA.102.052617>.
- [29] S. Ebadi, A. Keesling, M. Cain, T. T. Wang, H. Levine, D. Bluvstein, G. Semeghini, A. Omran, J.-G. Liu, R. Samajdar, et al., *Quantum optimization of Maximum Independent Set using Rydberg atom arrays*, Science **376**, 1209 (2022), URL <https://doi.org/10.1126/science.abo6587>.
- [30] M. Cain, S. Chattopadhyay, J.-G. Liu, R. Samajdar, H. Pichler, and M. D. Lukin, *Quantum speedup for combinatorial optimization with flat energy landscapes* (2023), arXiv:2306.13123.
- [31] B. F. Schiffer, D. S. Wild, N. Maskara, M. Cain, M. D. Lukin, and R. Samajdar, *Circumventing superexponential runtimes for hard instances of quantum adiabatic optimization*, Phys. Rev. Res. **6**, 013271 (2024), URL <https://link.aps.org/doi/10.1103/PhysRevResearch.6.013271>.
- [32] J. R. Finžgar, M. J. A. Schuetz, J. K. Brubaker, H. Nishimori, and H. G. Katzgraber, *Designing quantum annealing schedules using bayesian optimization*, Phys. Rev. Res. **6**, 023063 (2024), URL <https://link.aps.org/doi/10.1103/PhysRevResearch.6.023063>.
- [33] J. R. Finžgar, A. Kerschbaumer, M. J. Schuetz, C. B. Mendl, and H. G. Katzgraber, *Quantum-informed recursive optimization algorithms*, PRX Quantum **5**, 020327 (2024), URL <https://link.aps.org/doi/10.1103/PRXQuantum.5.020327>.
- [34] S. Perseguers, *Hardness-dependent adiabatic schedules for analog quantum computing* (2024), 2410.08995, URL <https://arxiv.org/abs/2410.08995>.
- [35] R. S. Andrist, M. J. A. Schuetz, P. Minssen, R. Yalovetzky, S. Chakrabarti, D. Herman, N. Kumar, G. Salton, R. Shaydulin, Y. Sun, et al., *Hardness of the maximum-independent-set problem on unit-disk graphs and prospects for quantum speedups*, Phys. Rev. Res. **5**, 043277 (2023), URL <https://link.aps.org/doi/10.1103/PhysRevResearch.5.043277>.
- [36] M. J. A. Schuetz, R. S. Andrist, G. Salton, R. Yalovet-



- zky, R. Raymond, Y. Sun, A. Acharya, S. Chakrabarti, M. Pistoia, and H. G. Katzgraber, *Quantum compilation toolkit for rydberg atom arrays with implications for problem hardness and quantum speedups* (2024), 2412.14976, URL <https://arxiv.org/abs/2412.14976>.
- [37] M.-T. Nguyen, J.-G. Liu, J. Wurtz, M. D. Lukin, S.-T. Wang, and H. Pichler, *Quantum optimization with arbitrary connectivity using Rydberg atom arrays*, PRX Quantum **4**, 010316 (2023), URL <https://link.aps.org/doi/10.1103/PRXQuantum.4.010316>.
- [38] A. G. de Oliveira, E. Diamond-Hitchcock, D. M. Walker, M. T. Wells-Pestell, G. Pelegrí, C. J. Picken, G. P. A. Malcolm, A. J. Daley, J. Bass, and J. D. Pritchard, *Demonstration of weighted-graph optimization on a rydberg-atom array using local light shifts*, PRX Quantum **6**, 010301 (2025), URL <https://link.aps.org/doi/10.1103/PRXQuantum.6.010301>.
- [39] M. MacMahon and D. Garlaschelli, *Community detection for correlation matrices*, Physical Review X **5** (2015), URL <https://doi.org/10.1103/PhysRevX.5.021006>.
- [40] S. Lamm, C. Schulz, D. Strash, R. Williger, and H. Zhang, *Exactly Solving the Maximum Weight Independent Set Problem on Large Real-World Graphs* (2019), pp. 144–158, <https://epubs.siam.org/doi/pdf/10.1137/1.9781611975499.12>, URL <https://epubs.siam.org/doi/abs/10.1137/1.9781611975499.12>.
- [41] J. Chen, I. A. Kanj, and W. Jia, *Vertex cover: Further observations and further improvements*, Journal of Algorithms **41**, 280 (2001), ISSN 0196-6774, URL <https://www.sciencedirect.com/science/article/pii/S0196677401911861>.
- [42] M. Sciorilli, L. Borges, T. L. Patti, D. García-Martín, G. Camilo, A. Anandkumar, and L. Aolita, *Towards large-scale quantum optimization solvers with few qubits*, Nature Communications **16**, 476 (2025), URL <https://doi.org/10.1038/s41467-024-55346-z>.
- [43] M. Dupont, B. Sundar, B. Evert, D. E. B. Neira, Z. Peng, S. Jeffrey, and M. J. Hodson, *Benchmarking quantum optimization for the maximum-cut problem on a superconducting quantum computer*, Phys. Rev. Appl. **23**, 014045 (2025), URL <https://link.aps.org/doi/10.1103/PhysRevApplied.23.014045>.
- [44] A. Acharya, R. Yalovetzky, P. Minssen, S. Chakrabarti, R. Shaydulin, R. Raymond, Y. Sun, D. Herman, R. S. Andrist, G. Salton, et al., *Decomposition pipeline for large-scale portfolio optimization with applications to near-term quantum computing* (2024), 2409.10301, URL <https://arxiv.org/abs/2409.10301>.
- [45] H. Karimi, G. Rosenberg, and H. G. Katzgraber, *Effective optimization using sample persistence: A case study on quantum annealers and various monte carlo optimization methods*, Phys. Rev. E **96**, 043312 (2017), URL <https://link.aps.org/doi/10.1103/PhysRevE.96.043312>.
- [46] S. Bravyi, A. Kliesch, R. Koenig, and E. Tang, *Obstacles to variational quantum optimization from symmetry protection*, Phys. Rev. Lett. **125**, 260505 (2020), URL <https://link.aps.org/doi/10.1103/PhysRevLett.125.260505>.
- [47] N. Mohseni, P. L. McMahon, and T. Byrnes, *Ising machines as hardware solvers of combinatorial optimization problems*, Nature Reviews Physics **4**, 363 (2022), URL <https://doi.org/10.1038/s42254-022-00440-8>.
- [48] C. S. Adams, J. D. Pritchard, and J. P. Shaffer, *Rydberg atom quantum technologies*, Journal of Physics B: Atomic, Molecular and Optical Physics **53**, 012002 (2019), URL <https://dx.doi.org/10.1088/1361-6455/ab52ef>.
- [49] M. D. Lukin, M. Fleischhauer, R. Cote, L. M. Duan, D. Jaksch, J. I. Cirac, and P. Zoller, *Dipole blockade and quantum information processing in mesoscopic atomic ensembles*, Phys. Rev. Lett. **87**, 037901 (2001), URL <https://link.aps.org/doi/10.1103/PhysRevLett.87.037901>.
- [50] M. Saffman, T. G. Walker, and K. Mølmer, *Quantum information with Rydberg atoms*, Rev. Mod. Phys. **82**, 2313 (2010), URL <https://link.aps.org/doi/10.1103/RevModPhys.82.2313>.
- [51] H. Levine, A. Keesling, G. Semeghini, A. Omran, T. T. Wang, S. Ebadi, H. Bernien, M. Greiner, V. Vuletić, H. Pichler, et al., *Parallel implementation of high-fidelity multiqubit gates with neutral atoms*, Phys. Rev. Lett. **123**, 170503 (2019), URL <https://link.aps.org/doi/10.1103/PhysRevLett.123.170503>.
- [52] J. Wurtz, A. Bylinskii, B. Braverman, J. Amato-Grill, S. H. Cantu, F. Huber, A. Lukin, F. Liu, P. Weinberg, J. Long, et al., *Aquila: Quera's 256-qubit neutral-atom quantum computer* (2023), arXiv:2306.11727.
- [53] K. Kim, M. Kim, J. Park, A. Byun, and J. Ahn, *Quantum computing dataset of maximum independent set problem on king lattice of over hundred rydberg atoms*, Scientific Data **11**, 111 (2024), URL <https://doi.org/10.1038/s41597-024-02926-9>.
- [54] A. Holtzman, J. Buys, L. Du, M. Forbes, and Y. Choi, *The curious case of neural text degeneration* (2020), 1904.09751, URL <https://arxiv.org/abs/1904.09751>.
- [55] H. Neven, *Meet willow, our state-of-the-art quantum chip* (2024), URL <https://blog.google/technology/research/google-willow-quantum-chip/>.
- [56] J. S. Otterbach, R. Manenti, N. Alidoust, A. Bestwick, M. Block, B. Bloom, S. Caldwell, N. Didier, E. S. Fried, S. Hong, et al., *Unsupervised machine learning on a hybrid quantum computer* (2017), 1712.05771, URL <https://arxiv.org/abs/1712.05771>.
- [57] M. P. Harrigan, K. J. Sung, M. Neeley, K. J. Satzinger, F. Arute, K. Arya, J. Atalaya, J. C. Bardin, R. Barends, S. Boixo, et al., *Quantum approximate optimization of non-planar graph problems on a planar superconducting processor*, Nature Physics **17**, 332 (2021), URL <https://doi.org/10.1038/s41567-020-01105-y>.
- [58] G. Pagano, A. Bapat, P. Becker, K. S. Collins, A. De, P. W. Hess, H. B. Kaplan, A. Kyprianidis, W. L. Tan, C. Baldwin, et al., *Quantum approximate optimization of the long-range ising model with a trapped-ion quantum simulator*, Proceedings of the National Academy of Sciences **117**, 25396 (2020), <https://www.pnas.org/doi/pdf/10.1073/pnas.2006373117>, URL <https://www.pnas.org/doi/abs/10.1073/pnas.2006373117>.
- [59] Z. He, R. Shaydulin, D. Herman, C. Li, R. Raymond, S. H. Sureshbabu, and M. Pistoia, *Parameter setting heuristics make the quantum approximate optimization algorithm suitable for the early fault-tolerant era* (2024), 2408.09538, URL <https://arxiv.org/abs/2408.09538>.
- [60] J. Wurtz and D. Lykov, *Fixed-angle conjectures for the quantum approximate optimization algorithm on regular maxcut graphs*, Phys. Rev. A **104**, 052419 (2021),



- URL <https://link.aps.org/doi/10.1103/PhysRevA.104.052419>.
- [61] B. Augustino, M. Cain, E. Farhi, S. Gupta, S. Gutmann, D. Ranard, E. Tang, and K. V. Kirk, *Strategies for running the qaoa at hundreds of qubits* (2024), 2410.03015, URL <https://arxiv.org/abs/2410.03015>.
- [62] M. W. Johnson, M. H. S. Amin, S. Gildert, T. Lanting, F. Hamze, N. Dickson, R. Harris, A. J. Berkley, J. Johansson, P. Bunyk, et al., *Quantum annealing with manufactured spins*, *Nature* **473**, 194 (2011), URL <https://doi.org/10.1038/nature10012>.
- [63] A. del Campo, *Shortcuts to adiabaticity by counterdiabatic driving*, *Phys. Rev. Lett.* **111**, 100502 (2013), URL <https://link.aps.org/doi/10.1103/PhysRevLett.111.100502>.
- [64] M. Ohkuwa, H. Nishimori, and D. A. Lidar, *Reverse annealing for the fully connected p-spin model*, *Phys. Rev. A* **98**, 022314 (2018), URL <https://link.aps.org/doi/10.1103/PhysRevA.98.022314>.
- [65] R. Ghosh, L. A. Nutricati, N. Feinstein, P. A. Warburton, and S. Bose, *Exponential speed-up of quantum annealing via n-local catalysts* (2024), 2409.13029, URL <https://arxiv.org/abs/2409.13029>.
- [66] L. A. Nutricati, R. Ghosh, N. Feinstein, S. Bose, and P. A. Warburton, *Enhancing the energy gap of random graph problems via xx-catalysts in quantum annealing* (2024), 2409.16350, URL <https://arxiv.org/abs/2409.16350>.

## Appendix A: Additional Details

Here we provide further details for the qReduMIS algorithm. We first discuss variants of qReduMIS, such as a *quantum-frugal* version to speed-up the algorithmic run time. Thereafter, we show how to implement qReduMIS across different quantum hardware platforms, including superconducting qubits and trapped ions.

### 1. Algorithmic Details for qReduMIS

**Anatomy of qReduMIS.** The qReduMIS algorithm is sketched in Algorithm 1. Here, we provide some more details for its implementation. In each iteration, qReduMIS updates the set of selected nodes  $\mathcal{S}$  that tracks nodes selected per classical reduction as well as nodes selected as (frozen) in-set kernel nodes. In parallel, the incumbent  $\mathcal{W}$  is also updated in every iteration whenever a better solution has been found, allowing us to track (potentially high-quality) global solution candidates already in the first iteration, even when the kernel  $\mathcal{K}$  may still be relatively large and  $|\mathcal{S}|$  relatively small. As such, the QPU’s output in the form of candidate sets  $\{\mathcal{I}_n\}$  is used in two ways, to establish a global incumbent solution and to identify frozen nodes as to unblock the kernelization process. In this way qReduMIS proceeds towards large independent sets in two complementary ways, with the incumbent  $\mathcal{W}$  securing a global solution candidate even when the algorithm is stopped early.

**Variants of qReduMIS.** For  $\lambda = K_{\text{RCL}} = 1$  the semi-greedy implementation of qReduMIS discussed in the main text simplifies to a simple greedy variant of qReduMIS. Generalizations of our semi-greedy implementation (with uniform random sampling from top- $K$  candidates) to alternative sampling strategies, such as top- $p$  (nucleus) sampling [54], should be straightforward. In semi-greedy qReduMIS with  $R$  parallel runs (repetitions) the total number of QPU calls amounts to  $N_{\text{QPU}} \sim R \cdot D$ . However, this number can be reduced to  $N_{\text{QPU}} \sim D$  in a *quantum-frugal* variant of qReduMIS, whereby the inexpensive classical reduction is run for all candidate nodes in the restricted candidate list RCL (as to validate multiple scenarios based on quantum information) before one greedily uses the option with the largest reduction footprint.

**qReduMIS run time.** The qReduMIS run time may be further reduced by keeping the number of shots  $n_{\text{shots}}$  low, because high-resolution measurements are not necessarily required, akin to the use of stochastic gradient descent over gradient descent. Moreover, the run time depends heavily on the quantum device used and its characteristic cycle time  $\tau$ . For Rydberg atom arrays, we currently have relatively slow cycle times with  $\tau \sim 0.1\text{s}$ , amounting to  $\sim 10$  samples per second. Conversely, with superconducting devices one can achieve more than  $6 \times 10^4$  circuit repetitions per second [55], resulting in much faster cycle times with  $\tau \sim 1.6 \times 10^{-5}\text{s}$ .

**Robustness.** By design, qReduMIS is robust against errors in that it can succeed in finding the MIS for the original input  $\mathcal{G}$  even if the QPU fails to find the MIS for the kernels  $\mathcal{K}$ , as long as the in-set (or out-set) classification suggested by the QPU is compatible with some MIS solution. For typical, sufficiently dense problems of interest, the majority of vertices will be out-set nodes resulting in an imbalanced classification problem in which the correct prediction of some out-set nodes is expected to be easier than the correct prediction of in-set nodes. For example, for the instances studied in Tab. I with  $n = 137$  and typical MIS size of  $\sim 46$  the average in-set probability is approximately  $\bar{p}_{\text{in}} \sim 1/3$ , while the average out-set probability is approximately  $\bar{p}_{\text{out}} \sim 2/3$ . However, removal of in-set nodes comes with a larger reduction footprint and thus typically requires a smaller number of qReduMIS iterations. Empirically, we observe that the two effects roughly balance each other out, leading to approximately similar performance for in-set and out-set selection strategy. We leave a more detailed analysis thereof, along with the development and analysis of alternative selection strategies, for future research.

**Loading errors.** In particular, qReduMIS can also improve the robustness against atom loading errors for Rydberg devices. Specifically, for the QuEra Aquila device, the typical probability of failing to occupy a given (single) site is  $\epsilon \sim 0.007$  [52]. The probability to correctly load a desired atom arrangement with  $n$  atoms is then  $p_{\text{load}} \approx (1 - \epsilon)^n$ . We have addressed this source of error through proper post-selection, noting that the fraction of valid samples can be much larger for qReduMIS over QAA, given that the kernel graph is typically much smaller than the original graph. For example, for the hardest instance in Tab. I, we have  $p_{\text{load}} \sim 38\%$  for QAA with  $n = 137$ , while  $p_{\text{load}} \sim 77\%$  for correctly loading the (first) kernel with  $n = 37$  nodes within qReduMIS.

### 2. Hardware Layer

The qReduMIS framework is hardware-agnostic. In the main text we have focused on implementations based on Rydberg atom arrays. Here, we now show how qReduMIS could be backed by digital (gate-based) devices run, for example, on superconducting (SC) qubits or trapped ions, or alternative SC-based quantum annealers. In order to use these backends within the qReduMIS framework, one needs to specify the unitary  $\mathcal{U}(\theta)$  that implements the desired dynamics in Eq. (3). Below, we describe this process for both the quantum approximate optimization algorithm using digital architectures, and quantum annealing using superconducting qubits.

**QAOA.** The quantum approximate optimization algorithm (QAOA) is one of the most widely studied quantum algorithms for solving combinatorial optimization problems on *gate-based*, near-term quantum devices [24], with first experimental demonstrations run on both superconducting qubits [56, 57] and trapped ions [58]. In

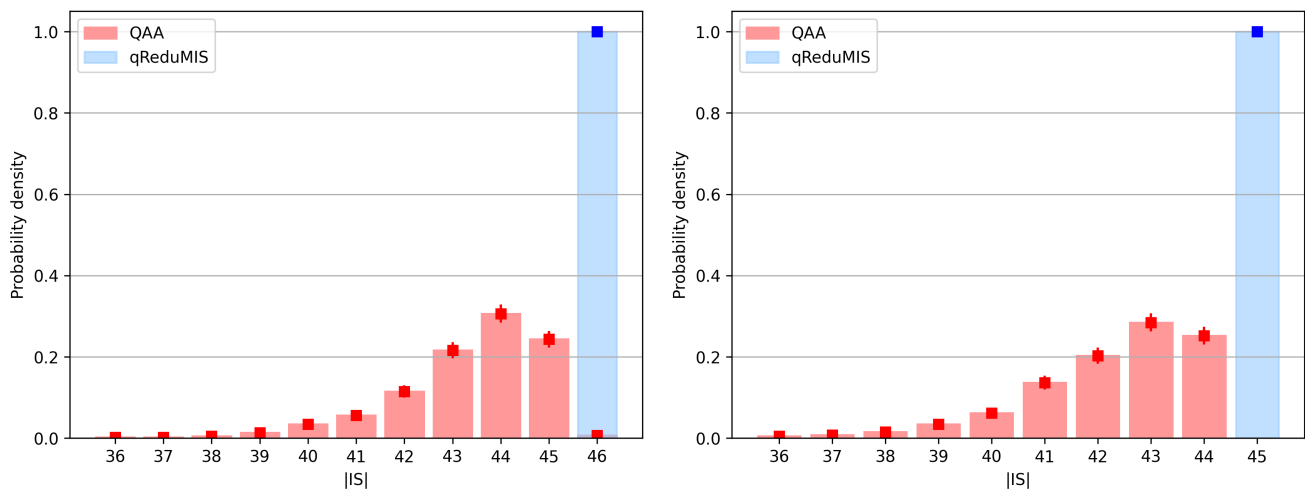


FIG. 4: Performance as measured in terms of the independent set size  $|\text{IS}|$  for both QAA and qReduMIS (with in-set selection) for the two hardest instances considered in Tab. I with  $\mathbb{H} \sim 125.5$  (left) and  $\mathbb{H} \sim 1435$  (right), respectively. The optimal MIS sizes are given in the rightmost bin. **(Left)** QAA finds the optimum  $|\text{MIS}| = 46$  with a small success rate of  $P_{\text{MIS}} \sim 0.7\%$ , displaying a broad shoulder towards suboptimal solutions, while qReduMIS finds the optimum with a success rate of  $P_{\text{MIS}} = 100\%$ . **(Right)** The best solution found by QAA is  $|\text{IS}| = 44$ , while qReduMIS finds the MIS of size  $|\text{MIS}| = 45$  with a success rate of  $P_{\text{MIS}} = 100\%$ . Error bars refer to 90% confidence intervals as extracted via bootstrapping, and  $n_{\text{shots}} = 1000$  for all QPU calls.

the case of QAOA, the unitary  $\mathcal{U}(\theta)$  in Eq. (3) is given by  $\mathcal{U}(\theta) = \prod_{l=1}^p U_{\text{mix}}(\beta_l) U_{\text{cost}}(\gamma_l)$ , involving a series of  $p$  layers alternating cost and mixing unitaries,  $U_{\text{cost}}(\gamma_l) = \exp(-i\gamma_l \hat{H}_{\text{cost}})$  and  $U_{\text{mix}}(\beta_l) = \exp(-i\beta_l \hat{H}_{\text{mix}})$ , respectively, which are generated by  $\hat{H}_{\text{cost}}$  and  $\hat{H}_{\text{mix}} = \sum_i \hat{X}_i$ , respectively. The parameters  $\theta = (\gamma, \beta)$  can either be optimized in an outer (closed) loop, inferred from parameter setting heuristics [25, 59, 60], or pre-optimized [61]. Finally, note that one could also adopt generalizations of QAOA such as recursive QAOA (RQAOA) [46].

**Superconducting annealers.** Alternatively, when adopting superconducting (SC) quantum annealers, e.g., as provided by D-Wave Systems Inc. [19, 22, 23, 62], the unitary  $\mathcal{U}(\theta)$  in Eq. (3) is generated by the time-dependent Hamiltonian  $\hat{H}(t) = (1 - \theta)\hat{H}_{\text{mix}} + \theta\hat{H}_{\text{cost}}$ , where  $\theta = \theta(t)$  defines the annealing schedule with  $\theta(0) = 0$  and  $\theta(\tau_f) = 1$  for a total anneal time  $\tau_f \sim 10\mu\text{s}$ . More general protocols can involve techniques such as counterdiabatic driving [63], reverse annealing [64], Bayesian optimization [32], or catalyst terms [65, 66].

## Appendix B: Additional Numerical Results

In this Appendix, we provide further details for our hardware experiments and additional numerical results, complementing the results shown in the main text.

**Algorithm parameters.** In our experiments we have set  $\lambda = 1$ , and  $K_{\text{RCL}} = 0.4|\mathcal{K}|$ , where  $|\mathcal{K}|$  refers to the number of kernel nodes. Measurements have been filtered to solution candidates  $\{\mathcal{I}_n\}$  with the largest and second largest independent set size found.

TABLE II: Success probabilities  $P_{\text{MIS}}$  (including error estimates) achieved with QAA and qReduMIS (for both an in-set and out-set selection strategy) using the QuEra Aquila QPU [52] for four test instances (all with  $n = 137$  vertices) referenced by their hardness parameters  $\mathbb{H}$ .

| Algorithm          | $\mathbb{H} \sim 1.478$ | $\sim 14.12$ | $\sim 125.5$ | $\sim 1435$ |
|--------------------|-------------------------|--------------|--------------|-------------|
| QAA                | 0.35(2)                 | 0.008(5)     | 0.007(4)     | 0.0         |
| qReduMIS (out-set) | 1.0                     | 1.0          | 1.0          | 1.0         |
| qReduMIS (in-set)  | 1.0                     | 1.0          | 1.0          | 1.0         |

**Hardware parameters.** For our hardware experiments we adopt the optimized schedules developed in Ref. [34], with a maximum Rabi frequency  $\Omega_{\text{max}}/2\pi = 2.5\text{MHz}$  and total annealing time  $\tau_f = 4\mu\text{s}$ . The lattice spacing  $a$  was set to  $a = 5.45\mu\text{m}$  for most of the problem instances, ensuring that the Rydberg blockade radius  $R_b \equiv (C_6/\Omega_{\text{max}})^{1/6}$  is compatible with the desired UJ connectivity, i.e.,  $\sqrt{2} \leq R_b/a < 2$  for  $R_b/a \sim 1.5$ . Given device geometry constraints in the form of limited maximum site pattern width and height [52], for large instances we set  $a = (4.45 - 5.0)\mu\text{m}$  when necessary, amounting to  $R_b/a \sim 1.7 - 1.9$ , well within the desired UJ regime.

**Example instances.** We first provide an extended version of Tab. I that features error bars (as extracted from bootstrapping) and provides results for both in-set and out-set selection strategies; see Tab. II. We observe comparable performance for the two selection strategies. In addition, complete histograms featuring all shots (QAA) and repetitions (qReduMIS) for the two hardest

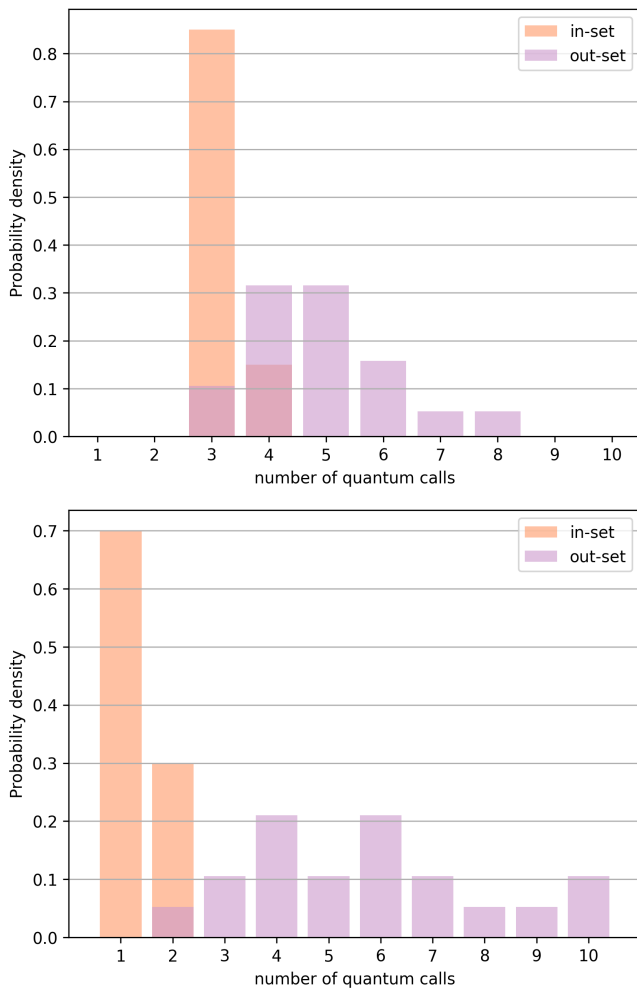


FIG. 5: Number of QPU calls for both in-set and out-set selection strategy (with  $\lambda = 1$ ) for the two hardest instances considered in Tab. I with  $\mathbb{H} \sim 125.5$  (top) and  $\mathbb{H} \sim 1435$  (bottom), respectively.

instances considered in Tab. I are displayed in Fig. 4. We see that with qReduMIS the probability is shifted to larger independent set sizes, indicating that performance is improved not only in the best case, but also on average.

**Number of QPU calls.** In Fig. 5, we provide histograms showing the number of QPU calls (across  $R = 20$  runs) for both in-set and out-set selection strategies for the two hardest instances considered in Tab. I. We find that a small number of calls ( $\lesssim 10$ ) is sufficient for these instances with  $n = 137$  nodes, in line with the expected (moderate) logarithmic increase of algorithmic depth  $D$  with system size  $n$ . Moreover, we find that in-set selection typically requires a smaller number of QPU calls, likely due to its larger removal footprint, because we only

remove one (frozen) node at a time (for  $\lambda = 1$ ) within the out-set strategy, but we remove one frozen node together with its kernel neighborhood when adopting the in-set strategy. As such, qReduMIS is expected to reach an empty kernel faster when adopting the in-set strategy.

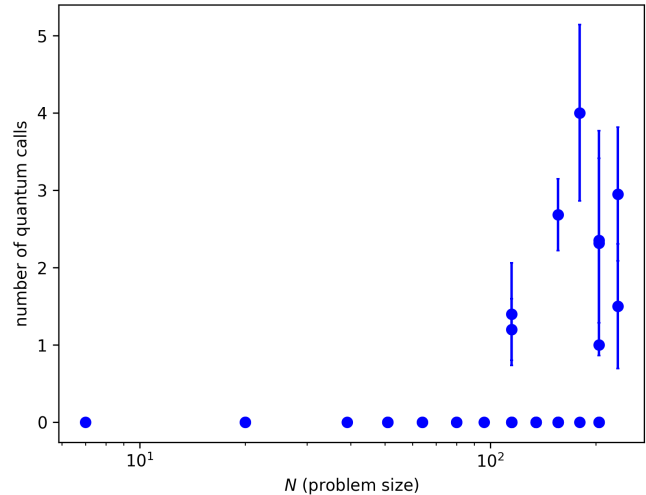


FIG. 6: Number of QPU calls for qReduMIS with in-set selection across the larger testbed with 39 instances with up to 231 nodes.

Finally, we note that the number of QPU calls can be reduced with a simple extension of our selection strategy in which we select one node per kernel component which allows to (potentially) unblock all kernel components in parallel.

Likewise, the number of QPU calls for qReduMIS with in-set selection across the larger testbed underlying Fig. 3 is shown in Fig. 6. We find that small UJ instances with  $n \lesssim 100$  nodes tend to be fully reducible, and thus do not require any QPU calls [36]. Some of the larger instances with  $n \gtrsim 100$  nodes may have a non-empty kernel, and thus may require calls to the QPU. However, compared to vanilla QAA, the overhead is small in that a small number of calls is sufficient to reach termination of qReduMIS.

We also observe a relatively strong Pearson correlation coefficient  $\sim -0.92$  between the number of QPU calls and the size of the first reduction, i.e., the larger the first classical reduction, the smaller the average number of QPU calls. The number of QPU calls is anti-correlated with the performance measure  $P_{\text{MIS}}$ , as confirmed by a relatively strong Pearson correlation coefficient of  $\sim -0.40$ . Overall, the emerging rationale can be simply stated as follows: The larger the problem size  $n$ , the smaller the average reduction, the larger the kernel, the larger the number of QPU calls, the smaller the average  $P_{\text{MIS}}$ .